RSC Advances

PAPER

View Article Online
View Journal | View Issue

Cite this: *RSC Adv.*, 2021, **11**, 14121

Kinetics of the gas-phase reaction of hydroxyl radicals with trimethyl phosphate over the 273–837 K temperature range

P. V. Koshlyakov,[a] D. A. Barkova,[a] I. E. Gerasimov,[a] E. N. Chesnokov,[a]* Xiaokai Zhang[b] and L. N. Krasnoperov*[b]

The kinetics of the reaction of hydroxyl radical (OH) with trimethyl phosphate $(CH_3O)_3PO$ (TMP) (reaction (1)) OH + TMP → products (1) was studied at the bath gas (He) pressure of 1 bar over the 273–837 K temperature range. Hydroxyl radicals were produced in fast reactions of electronically excited oxygen atoms $O(^1D)$ with either H_2O or H_2. Excited oxygen atoms $O(^1D)$ were produced by photolysis of ozone, O_3, at 266 nm (4th harmonic of Nd:YAG laser) over the 273–470 K temperature range and by photolysis of N_2O at 193 nm (ArF excimer laser) over the whole temperature range including the elevated temperature range 470–837 K. The reaction rate constant exhibits a V-shaped temperature dependence, negative in the low temperature range, 273–470 K (the rate constant decreases with temperature), and positive in the elevated temperature range, 470–837 K (the rate constant increases with temperature), with a turning point at 471 K. The rate constant could be fairly well fitted with the three parameter modified Arrhenius expression, $k_1 = 7.52 \times 10^{-18}$ (T/298)^9 exp(34 367 J mol^{-1}/RT) cm^3 per molecule per s (273–837 K). Previously, only one indirect experimental measurement at a single (ambient) temperature was available. The temperature dependence over an extended temperature range obtained in this study together with the peculiar V-shaped temperature dependence will have an impact on the modelling of the flame inhibition by phosphates as well on the further understanding of the mechanisms of elementary chemical reactions.

Received 3rd February 2021
Accepted 8th April 2021

DOI: 10.1039/d1ra00911g

rsc.li/rsc-advances

Introduction

Extinguishing fires can be achieved either *via* physical methods dilution such as dilution of air with inert gases, such as nitrogen, carbon dioxide, or water, or hindering the access of oxygen by solid powders, foams, or water vapor, to reduce oxygen concentration in the reaction zone, or by the addition of chemicals (flame retardants) which consume the active reactive species in the combustion processes. The second approach is more promising, since the flame inhibitors could be efficient even at low concentrations.[1]

After chlorofluorocarbons (CFCs) were banned by the Montreal Protocol in 1987, organophosphorus compounds were recognized as the most promising chemically active flame retardants.[2] Trimethyl phosphate (TMP) (the trimethyl ester of phosphoric acid) is perhaps one of the most famous chemical compounds of this class. For reliable assessment of the efficacy of chemically active flame inhibitors and required quenching concentrations, detailed chemical combustion mechanisms that include reactions of the active intermediates with the additives are required. First experimental studies on the kinetics of doped flames were conducted by Hestie[3] and Twarowski.[4–7] In these studied kinetic mechanisms have been proposed that formed the basis for further developments. Numerical and experimental studies of the combustion of TMP were carried out by several research groups.[8–12] Based on these and other studies, a mechanism for the destruction of organophosphorus compounds in combustion systems was proposed,[13] which included the maximum possible number of various intermediate products, as well as quantum-chemical *ab initio* calculations of all key elementary chemical reactions performed (using the BAC-G2 method).

It should be noted, however, that the main focus of these initial studies was on the pathways of the conversion of phosphorus-containing compounds themselves mainly *via* involvement in the catalytic recombination of free radicals, the process responsible for flame inhibition. The rate constants of the reactions of TMP with the free radicals have been only estimated, and certainly require accurate and detailed experimental determinations.

Surprisingly, current kinetic experimental as well as theoretical studies on the elementary reactions of free radicals even

[a]*Institute of Chemical Kinetics and Combustion, Siberian Branch of Russian Academy of Sciences, Novosibirsk, 630090, Russian Federation. E-mail: chesnokov@kinetics.nsc.ru*

[b]*Department of Chemistry and Environmental Science, New Jersey Institute of Technology, Newark, NJ 07102, USA. E-mail: lev.n.krasnoperov@njit.edu*

for the most widely used organophosphorus flame retardant, TMP, are very sparse. Even for the reaction of the most reactive hydroxyl radical, the major chain carrier species, in combustion, with TMP, there is only one measurement. There is only one experimental work[14] devoted to the measurement of the rate constant OH + TMP (reaction (1)):

$$OH + TMP \rightarrow \text{products} \quad (1)$$

In this study,[14] the rate constant was measured using indirect relative rates method (relative to the reaction OH + $(CH_3)_2O$) at a single temperature (ambient). The measured rate constant is $k_1 = 7.41 \times 10^{-12}$ cm^3 per molecule per s at 295 K. In the only one theoretical work[15] the potential energy surface (PES) for reaction (1) was characterized using quantum chemistry, with subsequent application of the transition state theory and only the channels associated with H-atom abstraction were evaluated. No information on the importance of the pathways *via* attachment of OH to the double P═O bond is currently available. No information on the possible pressure dependence of the rate constant of reaction (1) either experimental or theoretical exists. The scarceness of the information associated with the kinetics, temperature and pressure dependences, the pass ways and the products of reaction (1) warrants further extended experimental (desirably direct) and theoretical studies.

In this paper, we report a direct measurement of the reaction rate constant OH + TMP (reaction (1)) by laser flash photolysis combined by transient UV absorption spectroscopy over an extended temperature range 273–837 K.

The measurements were performed in two laboratories (Institute of Chemical Kinetics and Combustion, IChK&C, Novosibirsk, Russia) and (New Jersey Institute of Technology, NJIT, Newark, USA). In both studies hydroxyl radicals (OH) were formed using fast reaction of electronically excited atoms O(^{1}D) with either H_2O or H_2 molecules:[16]

$$O(^1D) + H_2O \rightarrow 2OH \quad (2a)$$

$$O(^1D) + H_2 \rightarrow OH + H \quad (2b)$$

Both reactions are very fast, the reaction of O(^{1}D) with H_2O requires only a few collisions (the rate constant $k_{(2a)} = 2.0 \times 10^{-10}$ cm^3 per molecule per s at 298 K).[16] Moreover, due to the relatively strong O–H bond in water molecule, reaction (2a) produces fewer vibrational and rotational excitations, compared to reaction (2b), or any other reaction with H-containing molecules. Therefore, the majority of the measurements, were performed using reaction (2a) to generate hydroxyl radicals. Reaction (2b) was used in several experiment to verify the stability of the results.

At the Institute of Chemical Kinetics and Combustion, (IChK&C), electronically excited oxygen atoms were produced by photolysis of ozone at 266 nm:

$$O_3 + h\nu\ (266\ \text{nm}) \rightarrow O(^1D) + O_2 \quad (3)$$

The temperature range of this study was 273–470 K, the highest temperature was limited by the thermal stability of ozone. Even though the relatively narrow temperature range of the study using photolysis of ozone, the results indicated that the temperature dependence is probably V-shaped, *i.e.*, the rate constant decreases with temperature at low temperatures, and increases at higher temperatures. Therefore the decision was made to significantly expand the temperature range using a different photolysis system, available at NJIT. Specifically, to produce excited oxygen atoms, photolysis of N_2O at 193 nm (ArF excimer laser). N_2O has much better thermal stability, compared with that of ozone. The replacement of excited oxygen atom photochemical precursor, allowed raising the upper temperature of the available temperature range to 837 K.

$$N_2O + h\nu\ (193\ \text{nm}) \rightarrow O(^1D) + O_2 \quad (4)$$

Experimental

With the exception of the different photolysis techniques of generation of electronically excited oxygen atoms, the experimental approaches used at the IChK&C and NJIT are almost identical. In both cases, pulsed laser photolysis, coupled with the time-resolved transient UV absorption was used.

The experimental set-up at IChK&C was partially described previously.[17] The sketch of the set-up is shown in Fig. 1. Fig. 1, experimental set up at the Institute of Chemical Kinetics and Combustion. Ozone is photolyzed at 266 nm (4th harmonic of an Nd:YAG laser, Lotis Tii, model: LS-2137U). Temporal profiles of OH absorption of light produced by a DC discharge hydroxyl lamp (multiline around 308 nm) passed through a monochromator are digitized, accumulated and stored using a digital oscilloscope.

Ozone is produced in an on-line ozonator and mixed with other reactants in a flow system before entering a heatable flow reactor. The ozonator is made of quartz tube with a coaxial stainless steel rod inside. The quartz tube is wrapped with grounded aluminum foil. High AC voltage (50 Hz, 11 kV) is applied to the foil and the inner electrode. Gas mixture 10% of O_2 in He is mixed with the other reactants after passing the ozonator. Typical degree of conversion of O_2 to O_3 was about 7%. The ozone concentration in the reactor was determined accurately and directly *in situ* by absorbance at the 253 nm using mercury resonance lamp using accurately known absorption coefficients. Typical concentration of ozone was *ca.* 9.6×10^{14} molecule per cm^3 molecules. Typical concentration of molecular oxygen, O_2, was *ca.* 8×10^{15} cm^{-3}. Hydroxyl radicals were generated in two ways. The first method is in the reaction of an excited oxygen atom O(^{1}D) with water molecules (reaction (2a)) (the majority of the experiments) or with hydrogen molecules (reaction (2b)). Typical concentrations of water molecules was *ca.* 3×10^{16} molecule per cm^3 and of H_2 molecules *ca.* 3.7×10^{16} molecule per cm^3.

Hydroxyl radicals were monitored *via* absorption of light generated by a low pressure DC discharge lamp in a H_2O/Ar mixture. The OH lamp is a quartz tube, with two metal fittings at the ends. Argon, saturated with water vapor at pressure *ca.* 1 bar and ambient temperature, was pumped through the lamp at 40 torr. DC voltage of 5 kV was applied to the metal

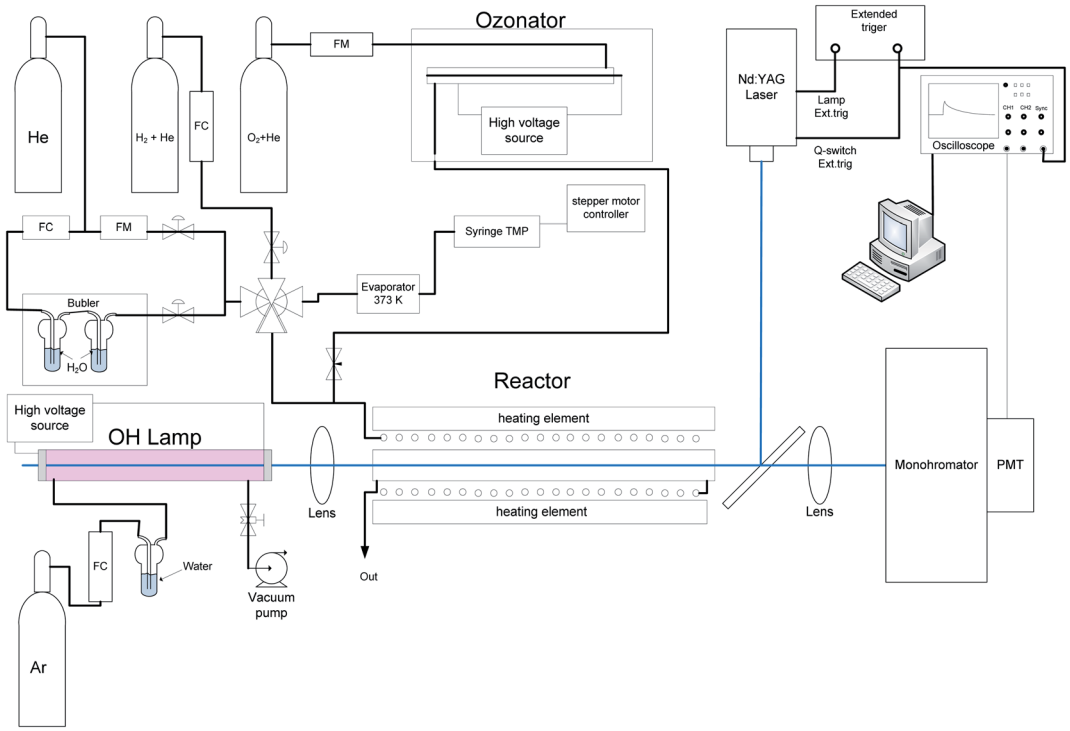

Fig. 1 Experimental set up at the Institute of Chemical Kinetics and Combustion. Ozone is produced in an on-line ozonator and mixed with other reactants before entering a heatable reactor. Ozone is photolysed by 4th harmonic of an Nd:YAG laser (266 nm). Temporal profiles of OH absorption of light produced by a DC discharge hydroxyl lamp (multiline around 308 nm) passed through a monochromator are digitized, accumulated and stored using a digital oscilloscope.

fittings of the OH lamp *via* a ballast resistor, the electric current was 30 mA. The light emitted from the lamp passed through the reactor was focused on the entrance slit of the monochromator (Carl Zeiss, SPM2). The spectral width was set *ca.* 12 nm to select a bunch of *ca.* 20 emission lines of hydroxyl radical around 308 nm. The temperature and pressure dependences of the apparent absorption cross-section of hydroxyl radical obtained with such a lamp as well as the curves-of-growth were studied in details in the experiments as well as *via* modeling in previous studies[17–20] For the optical arrangement, used in the current study, the low pressure low absorbance (<2%) experimentally determined apparent absorption cross section of OH was 7.2×10^{-17} cm^2 per molecule at 293 K.

A heated metal flow reactor was 10 cm long with an inner diameter of 8 mm with fused quartz windows was used. Before entering the heated reactor the flowing reaction mixture was pre-heated to the reactor temperature *via* placing the 2 m entering tube as well as the reactor in a common heater. The temperature of the reactor ranged from 273 K to 473 K. The pressure in the cell was *ca.* 12–15 torr above ambient atmospheric pressure and was in the range 750–775 torr.

The main bath gas (helium) flow rate was measured with an SMC PFMV510-1 flow meter. The main flow rate was 1000 sccm. The flow rate of the O_2/He mixture was measured before entering the ozonator by a MF Matheson 8141 flow meter; the flow rate was *ca.* 4 sccm. Measurements and control of small helium flows passing through a two stage water saturator was done using a TylanFC 260 mass flow controller. This helium flow was about 44 sccm. In the experiments when hydrogen was used instead of water, the flow rate of mixture of H_2/He (mixing ratio of 1 : 20) was controlled using a TylanFC 260 mass flow controller. The flow rate of the H_2/He mixture was 43 sccm.

The reactant (trimethyl phosphate, TMP) was introduced using an Agilent chromatographic syringe with a volume of 25 μL driven by a stepper motor. TMP was supplied to the evaporator, which in turn was purged with the main helium flow. The flow rate of liquid TMP ranged from 0 to 0.45 μL min^{-1} which, after evaporation, corresponds to 0–0.082 sccm. The TMP concentration in the reactor was varied from 0 to 1.5×10^{15} cm^{-3}.

Reagents (IChK&C)

The purity of the gases used in the work were: He >99.995%, O_2 grade pure >99.95%, H_2O was deionized, the resistance 17 MOhm cm. Ar >99.999%. TMP was purchased from Aldrich, pure, >97%.

The experimental set-up used at NJIT is described in detail in previous publications.[17–19,21–23] Hydroxyl radicals were generated in pulsed photolysis of N_2O in the presence of water vapor at 193.3 nm (ArF excimer laser). The importance of different channels of the photodissociation process (reaction (4)) as well as of the subsequent reaction of O(^{1}D) with H_2O (reaction (2a)) are also discussed in details in the previous publications.[17–19,21–23]

The kinetics of hydroxyl radical decay was monitored by absorption in the UV (multiline at *ca.* 308 nm using low pressure H_2O/Ar DC discharge lamp. Before entering the reactor, the laser beam was formed (to provide uniformity) with a spherical

lenses. The beam uniformity across the reactor cross-section was ±7.3% from the mean value. The gas flow rates were controlled by mass flow controllers (Brooks, model 5850). The total flow rates of the reactant mixtures with helium were in the range 20–75 sccs. Additional flush flows to the reactor windows were in the range 4.5–10 sccs. Two precision syringe pumps (Harvard Apparatus, model PHD 4400) were used to inject liquid water and TMP/H_2O solution (the mole fraction of TMP in the range $x_{TMP} = (1.00–2.50) \times 10^{-2}$) through their corresponding capillary tubes into an evaporator (kept at 90 °C) and, subsequently, to the reactor. In this way, steady flows of H_2O and TMP vapor were achieved. The total flow rate of these two liquids were kept constant at each given temperature, ranges from 6 to 15 μL min^{-1}, provided approximately the same concentration of H_2O. The equivalent gas flow rate of TMP in standard cubic centimeters per minute (sccm) was calculated based on the volumetric flow rate of the solution and known molar concentration (molarity) of the solution based on the ideal gas law. Sample TMP/H_2O solution preparation: a 100 mL volumetric flask first is filled with *ca.* 60 mL of distilled water, then 14.65 mL TMP (97%, density = 1.197 g mL^{-1} at 25 °C, MW = 140.07) (*n*TMP = 0.1214 mol) is added and dissolved, distilled water is added with continuous mixing until the volume mark line. The molarity of the final solution is then 1.2114 M. After preparation the solution is degassed three times using freeze-pump-thaw procedure before using in the experiments.

The concentrations of the precursors used were $(2.08–3.08) \times 10^{17}$ (H_2O), $(1.11–2.36) \times 10^{16}$ (N_2O) and $(0–10) \times 10^{14}$ (TMP) molecules per cm^3. The absolute concentrations of OH radicals were determined based on the photon flux inside the reactor, the absorption cross-section of N_2O at 193.3 nm, and the efficiency of conversion of $O(^1D)$ atoms produced in the photolysis of N_2O to OH radicals. The absorption cross-section of N_2O is accurately known at 298 and 1 bar, at other conditions, the cross-sections of N_2O were measured in the previous works. The model used for the calculations of the efficiency of conversion of excited $O(^1D)$ atom to OH radicals as well as the *in situ* laser light actinometry are described in details in the previous studies.[17–19,21–23] The approach is based on the monitoring of ozone formation at 253.6 nm in the photolysis of $N_2O/O_2/N_2$ mixtures at 1 bar and 298 K. The photolysis laser photon fluence inside the reactor was varied in the range $(4–9) \times 10^{15}$ photons per cm^2 per pulse. The initial concentrations of hydroxyl radicals were in the range $(4–9) \times 10^{13}$ molecule per cm^3. All experiments were performed at pressure 1 bar (He) over the temperature range 298–837 K.

Reagents (NJIT)

Helium used in the experiments was BIP®Helium from air gas with 99.9999% purity with reduced oxygen content (<10 ppb). UHP oxygen was obtained from Matheson TriGas (99.98% purity). Certified mixture of N_2O in He (2.50%, accuracy ±2%) obtained from Matheson Tri-Gas was used. Purified water (Milli-Q®) with TOC less than 5 ppb) was degassed by freeze-pump-thaw cycles and used as a reactant supplied by a syringe pump (Harvard Apparatus PHD 4400) as well as in the low pressure H_2O/Ar discharge hydroxyl monitoring lamp. UHP Argon obtained from Matheson TriGas (99.999% purity) was used in the H_2O/Ar lamp.

Results

Sample OH absorption profiles obtained in the $O_3/O_2/H_2O$/TMP/He + 266 nm are shown in Fig. 2. The raise of the absorption in the figure corresponds to the formation of hydroxyl in reaction (2a). The reaction of $O(^1D)$ atoms with H_2O is extremely fast (the rate constant, $k = 1.8 \times 10^{-10}$ cm^3 s^{-1})[16] therefore, the conversion time of an excited oxygen atom does not exceed 1 μs.

Decay of the OH concentration is due to the different reactions of OH, including OH radical self reaction, decay on the walls as well as the target reaction with TMP. The secondary reactions of the products of reaction (1) also contribute to the decay rates. In contrast to our previous studies of elementary reactions of hydroxyl radical and other radical species, where a system of differential equations that corresponds to the reaction mechanism was numerically solved and the resulting profiles were fitted to the experimental, a simplified analysis was accepted in this work. For reaction (1), currently no information about the products, branching ratios, and the rate constants of subsequent reactions of the products of reaction (1), is available, and the previously used rigorous approach is not feasible. *In lieu* of the lack of a detailed reaction mechanism, no integrated kinetic decay curves could be obtained. Therefore, the method of the initial rates also widely used in chemical kinetics, was applied as described below.

After formation of hydroxyl radicals in reactions (2a) or (2b), the radicals are consumed in the target reaction (1) as well as in the side reactions discussed above. Therefore, at short times the rate of consumption is written as:

$$-\frac{1}{[OH]_0} \times \frac{d[OH]}{dt} \quad \text{at } t = 0,\ k' = k'_1 + k_0 \qquad \text{(E1)}$$

where k' is the "initial slope" rate constant, $k'_1 = k_1[TMP]$ is the pseudo-first order rate constant of the target reaction, and k_0 accounts for all other processes. In the evaluation of the initial slopes, the initial fractions of the decay curves should be properly fitted. There are numerous functions, including just

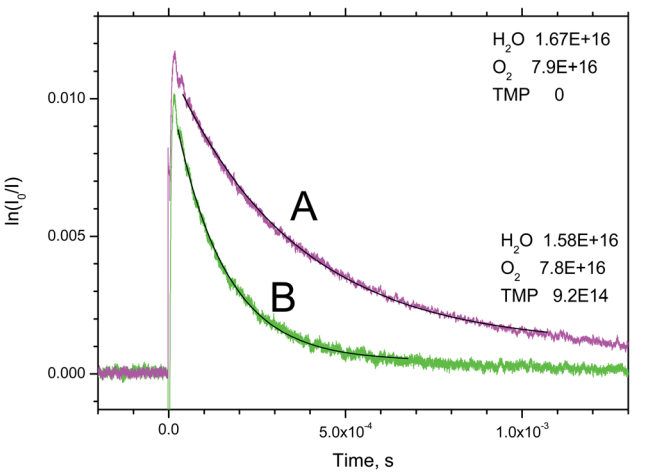

Fig. 2 Sample transient absorption signals of OH in $O_3/O_2/H_2O$/TMP/He mixtures. A – without TMP, B – [TMP] = 9.2×10^{14} molecule per cm^3.

the linear one, which can be used for this purpose. In the case of pseudo-first order decays, the decay profiles are exponential. Therefore, exponential decay function was chosen to evaluate the initial decay rates, since it provides unbiased estimation of the "initial slopes" for pseudo-first order processes.

To evaluate the "initial slope" rate constant, the initial portion of the decay profiles (about 1/3 of the amplitude) was fitted with exponential function

$$OH = [OH]_0 \times e^{-k't} \quad (E2)$$

Then plotting the "initial slope rate constant" *vs.* the reactant concentration [TMP] one expects to obtain a straight line which slope yields the rate constant of the target reaction (1), and the intercept the contribution of other processes (such as self reaction) at the initial stage of the reaction.

The rate constant of the self-reaction of hydroxyl radicals is well characterized,[17,19] and its contribution into the initial decay is easy assessable. Assessment of the potential interference of the reactions with the products of the target reaction (1) is not straightforward. The only possibility is to use very low initial concentrations of OH, to reduce the possible role of such processes. The maximum values of k' were about 20 000 s^{-1}. Assuming that the rate constants of the secondary reactions of OH with the presumable products of reaction (1) do not exceed typical value for barrierless radical–radical reactions of 3×10^{-11} cm^3 per molecule per s, an estimate can be made on the maximum concentrations of OH radicals to assure that the contribution of possible secondary reaction does not exceed 5% of the total decay, *i.e.*, 1000 s^{-1}, $[OH]_0 < 1000/3 \times 10^{-11} = 3 \times 10^{13}$ molecule per cm^3. For a cell length of 10 cm and the absorption cross-section of *ca.* 7×10^{-17} cm^2 per molecule, this concentration translates to the initial absorption of $3 \times 10^{13} \times 10 \times 7 \times 10^{-17} = 0.02$ (2%). Therefore, the majority of the experiments were performed with the initial absorbances in the range 0.3–2%.

Sample dependence of the "initial slope rate constant" k', on the reactant (TMP) concentration is shown in Fig. 3. The dependences are linear, the slopes yield the rate constants of the target reaction (1). The negative temperature dependence (the decrease of the reaction rate with temperature) is apparent in this (low) temperature range.

Additional experiments were performed using molecular hydrogen (instead of water) as the reactant to produce OH radicals in the reaction with $O(^1D)$, reaction (2b). Sample decay profiles are shown in Fig. 4. Longer rise time (compared to the experiments where water was used) is apparent. There are two reasons that contribute in the longer build-up times in the experiments with H_2 instead of water. First, reaction of excited oxygen atoms with molecular hydrogen produces relatively highly vibrationally excited OH radicals. The detection technique "sees" hydroxyl in the ground vibrational state. Therefore, vibrational relaxation of OH might contribute in the longer absorption build-up times. Second, the reaction that produces hydroxyl in this case (reaction (2b)), also produces H-atoms. These atoms subsequently produce additional OH radicals in reaction with ozone (reaction (5))

$$H + O_3 \rightarrow OH + O_2 \quad (5)$$

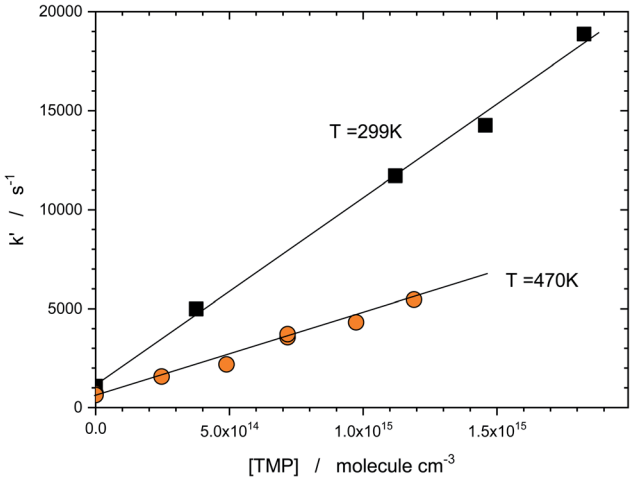

Fig. 3 Dependence of the "initial slope rate constant, k'" on concentration of TMP at two temperatures. The slope yields the rate constant of the target reaction (1). Negative temperature dependence (decrease of the rate constant with temperature) is apparent in this (low temperature) range.

The rate constant of this reaction is 3×10^{-11} cm^3 per molecule per s.[24] Under the experimental conditions of this work, the characteristic time of reaction (5) should be in the 30–50 μs range that roughly corresponds to the observed rise time. It should be noted that the reaction (5) has significant another channel (reaction (6)),[24] which further complicates the analysis of the build-up portion of the absorption profile:

$$H + O_3 \rightarrow HO_2 + O \quad (6)$$

Due to these reasons, no attempt was made to study quantitatively the build-up profiles. The measurements of the rate constant of the target reaction (1) were made in conditions when the build-up time is much shorter, than the

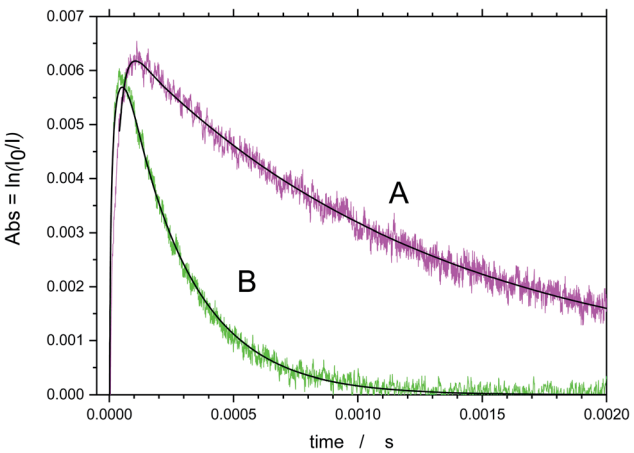

Fig. 4 Sample transient absorption signals of OH in $O_3/O_2/H_2/He$ mixture. A – without TMP, B – [TMP] = 3.6×10^{14} molecule per cm^3. Longer rise time (compared with the profiles where water was used) is apparent.

Table 1 Experimental condition for the experiments with $O_3/O_2/(H_2O$ or $H_2)$/TMP/He + 266 nm and N_2O/H_2O/TMP/He + 193 nm photolysis systems. All measurements at 1.00 ± 0.02 bar

T/K	$[N_2O]/10^{16}$ molecule per cm^3	$[O_3]/10^{14}$ molecule per cm^3	$[O_2]/10^{16}$ molecule per cm^3	$[H_2O]/10^{16}$ molecule per cm^3	$[H_2]/10^{16}$ molecule per cm^3	$[M]/10^{19}$ molecule per cm^3	$[TMP]/10^{15}$ molecule per cm^3	$k'/10^3$ s^{-1}	$k_1/10^{-12}$ cm^3 molecule per s
273	0	12.8	1.07	3.55	0	2.66	0	1.35	11.5
273	0	12.8	1.07	3.55	0	2.66	0	1.58	
273	0	12.8	1.08	3.64	0	2.66	0.507	8.26	
273	0	12.8	1.09	3.65	0	2.68	1.02	12.9	
273	0	12.8	1.09	3.64	0	2.69	1.52	13.4	
273	0	12.8	1.04	3.52	0	2.66	1.96	18.2	
273	0	12.8	1.05	3.51	0	2.68	2.44	17.7	
299	0	19.4	1.08	2.96	0	2.47	0	1.03	7.81
299	0	19.4	0.915	2.65	0	2.47	2.21	18.9	
299	0	19.4	0.992	2.70	0	2.47	0	1.09	
299	0	19.4	1.06	2.72	0	2.47	0.456	4.99	
299	0	19.4	0.994	2.70	0	2.47	1.36	11.7	
299	0	19.4	0.959	2.64	0	2.47	1.77	14.3	
328	0	9.42	0.952	2.85	0	2.25	0	0.840	5.16
328	0	9.42	1.01	2.97	0	2.25	2.21	12.3	
328	0	9.42	0.946	2.90	0	2.25	0.431	3.64	
328	0	9.42	0.950	2.88	0	2.25	0.855	5.41	
328	0	9.42	0.932	2.94	0	2.25	1.27	7.94	
328	0	9.42	0.898	2.87	0	2.25	1.66	9.71	
365	0	9.57	0.800	2.89	0	2.00	0	1.02	3.57
365	0	9.57	0.815	2.95	0	2.00	0.384	2.65	
365	0	9.57	0.842	2.94	0	2.00	0.767	3.76	
365	0	9.57	0.818	2.92	0	2.00	1.14	5.10	
365	0	9.57	0.781	2.86	0	2.00	1.49	6.58	
365	0	9.57	0.773	2.83	0	2.00	1.85	7.63	
411	0	7.80	0.753	2.52	0	1.78	0	0.926	2.86
411	0	7.80	0.753	2.52	0	1.78	0	1.27	
411	0	7.80	0.796	2.75	0	1.78	0.371	2.20	
411	0	7.80	0.789	2.76	0	1.78	0.744	3.40	
411	0	7.80	0.779	2.84	0	1.78	1.12	4.27	
411	0	7.80	0.771	2.83	0	1.78	1.44	5.21	
411	0	7.80	0.763	2.89	0	1.78	1.78	6.21	
470	0	6.44	0.651	2.28	0	1.57	0	0.526	2.77
470	0	6.44	0.651	2.28	0	1.57	0	0.521	
470	0	6.44	0.651	2.28	0	1.57	0	0.474	
470	0	6.44	0.641	2.34	0	1.57	0.299	1.52	
470	0	6.44	0.629	2.32	0	1.57	0.593	2.21	
470	0	6.44	0.637	2.34	0	1.57	0.870	3.52	
470	0	6.44	0.648	2.38	0	1.57	1.18	3.47	
470	0	6.44	0.634	2.33	0	1.57	1.44	4.55	
299	0	5.98	0.959	0	5.14	2.48	0	0.562	6.71
299	0	5.98	0.983	0	5.27	2.48	0.476	3.85	
299	0	5.98	0.973	0	5.22	2.48	0.941	6.67	
299	0	5.98	0.947	0	5.14	2.48	1.39	10.0	
299	0	5.98	0.914	0	5.03	2.48	1.81	11.1	
299	0	5.98	0.911	0	5.01	2.48	2.26	14.28	
273	0	8.53	1.12	0	5.63	2.75	0	1.85	11.5
273	0	8.53	1.20	0	5.98	2.75	0.546	11.1	
273	0	8.53	1.18	0	5.94	2.73	1.08	14.3	
273	0	8.53	1.16	0	5.83	2.71	1.6	16.6	
273	0	8.53	1.16	0	5.82	2.74	2.12	11.1	
273	0	8.53	1.14	0	5.77	2.73	2.64	14.28	
273	0	10.7	1.06	0	5.49	2.76	0	1.48	15.1
273	0	10.7	1.09	0	5.60	2.72	0.516	9.26	
273	0	10.7	0.911	0	5.58	2.74	1.03	10.96	
273	0	10.7	1.06	0	5.54	2.74	1.53	8.33	
273	0	10.7	1.03	0	5.44	2.74	2	18.55	
273	0	10.7	1	0	5.33	2.71	2.45	11.92	
328	0	7.78	0.905	0	4.56	2.28	0	1.40	6.45
328	0	7.78	0.905	0	4.56	2.28	0	0.813	

Table 1 (*Contd.*)

T/K	$[N_2O]/10^{16}$ molecule per cm^3	$[O_3]/10^{14}$ molecule per cm^3	$[O_2]/10^{16}$ molecule per cm^3	$[H_2O]/10^{16}$ molecule per cm^3	$[H_2]/10^{16}$ molecule per cm^3	$[M]/10^{19}$ molecule per cm^3	$[TMP]/10^{15}$ molecule per cm^3	$k'/10^3$ s^{-1}	$k_1/10^{-12}$ cm^3 molecule per s
328	0	7.78	0.978	0	4.76	2.28	0.440	3.95	
328	0	7.78	0.975	0	4.74	2.28	0.878	3.98	
328	0	7.78	0.961	0	4.73	2.28	1.31	6.25	
328	0	7.78	0.931	0	4.64	2.28	1.72	6.38	
328	0	7.78	0.913	0	4.6	2.28	2.12	10.53	
365	0	7.28	0.822	0	4.12	2.06	0	0.999	3.36
365	0	7.28	0.858	0	4.26	2.06	0.395	2.83	
365	0	7.28	0.858	0	4.27	2.06	0.790	3.97	
365	0	7.28	0.835	0	4.26	2.06	1.18	6.37	
365	0	7.28	0.847	0	4.28	2.06	1.58	6.20	
365	0	7.28	0.831	0	4.25	2.06	1.96	7.74	
411	0	5.30	0.771	0	3.80	1.82	0	0.82	2.93
411	0	5.30	0.752	0	3.76	1.82	0.346	1.83	
411	0	5.30	0.728	0	3.68	1.82	0.679	2.26	
411	0	5.30	0.703	0	3.65	1.82	1.01	3.92	
411	0	5.30	0.671	0	3.57	1.82	1.31	3.48	
411	0	5.30	0.641	0	3.50	1.82	1.61	4.48	
470	0	3.21	0.699	0	3.49	1.61	0	1.42	2.65
470	0	3.21	0.756	0	3.69	1.61	0.340	2.32	
470	0	3.21	0.624	0	3.19	1.61	0.589	2.82	
470	0	3.21	0.622	0	3.18	1.61	0.881	3.28	
470	0	3.21	0.621	0	3.18	1.61	1.17	3.38	
470	0	3.21	0.606	0	3.18	1.61	1.46	3.94	
300	0	7.14	0.934	3.53	0	2.40	0	1.22	7.90
300	0	7.14	0.904	3.68	0	2.39	0.432	4.76	
300	0	7.14	0.945	3.80	0	2.39	0.892	8.33	
300	0	7.14	0.947	3.99	0	2.39	1.34	11.1	
300	0	7.14	0.976	4.06	0	2.39	1.82	14.3	
300	0	7.14	0.964	4.00	0	2.39	2.25	20.0	
411	2.34	0	0	0	0	1.79	0	0.278	3.92
411	2.34	0	0	30.4	0	1.79	0.202	1.06	
411	2.34	0	0	30.4	0	1.79	0.405	1.89	
411	2.34	0	0	30.4	0	1.79	0.607	2.65	
411	2.34	0	0	30.4	0	1.79	0.809	3.25	
411	2.34	0	0	30.4	0	1.79	1.01	3.66	
673	1.62	0	0	0	0	1.09	0	0.397	5.28
673	1.62	0	0	29.8	0	1.09	0.199	1.78	
673	1.62	0	0	29.8	0	1.09	0.398	2.55	
673	1.62	0	0	29.8	0	1.09	0.597	3.38	
673	1.62	0	0	29.8	0	1.09	0.796	4.29	
673	1.62	0	0	29.8	0	1.09	0.995	4.88	
298	2.27	0	0	0	0	2.47	0	0.543	7.08
298	2.27	0	0	30.8	0	2.47	1.01	7.75	
298	2.27	0	0	30.8	0	2.47	0.811	6.41	
298	2.27	0	0	30.8	0	2.47	0.608	5.21	
298	2.27	0	0	30.8	0	2.47	0.406	3.72	
298	2.27	0	0	30.8	0	2.47	0.203	2.51	
298	2.27	0	0	0	0	2.47	0	0.529	
773	1.53	0	0	0	0	0.951	0	0.917	7.14
773	1.53	0	0	28.3	0	0.951	0.943	7.63	
773	1.53	0	0	28.3	0	0.951	0.754	6.02	
773	1.53	0	0	28.3	0	0.951	0.566	4.85	
773	1.53	0	0	28.3	0	0.951	0.377	3.30	
773	1.53	0	0	28.3	0	0.951	0.189	2.04	
673	1.66	0	0	0	0	1.10	0	0.599	5.28
673	1.66	0	0	30.6	0	1.10	1.02	5.99	
673	1.66	0	0	30.6	0	1.10	0.816	4.95	
673	1.66	0	0	30.6	0	1.10	0.612	3.95	
673	1.66	0	0	30.6	0	1.10	0.408	2.85	
673	1.66	0	0	30.6	0	1.10	0.204	1.73	
500	1.85	0	0	0	0	1.47	0	1.13	3.58

Table 1 (*Contd.*)

T/K	$[N_2O]/10^{16}$ molecule per cm^3	$[O_3]/10^{14}$ molecule per cm^3	$[O_2]/10^{16}$ molecule per cm^3	$[H_2O]/10^{16}$ molecule per cm^3	$[H_2]/10^{16}$ molecule per cm^3	$[M]/10^{19}$ molecule per cm^3	$[TMP]/10^{15}$ molecule per cm^3	$k'/10^3$ s^{-1}	$k_1/10^{-12}$ cm^3 molecule per s
500	1.85	0	0	29.6	0	1.47	1.02	4.74	
500	1.85	0	0	29.6	0	1.47	0.819	3.95	
500	1.85	0	0	29.6	0	1.47	0.614	3.28	
500	1.85	0	0	29.6	0	1.47	0.409	2.51	
500	1.85	0	0	29.6	0	1.47	0.205	1.67	
837	1.12	0	0	0	0	0.876	0	0.610	12.6
837	1.11	0	0	10.5	0	0.876	1.05	13.9	
837	1.11	0	0	20.8	0	0.876	0.833	10.7	
837	1.11	0	0	20.8	0	0.876	0.625	7.46	
837	1.11	0	0	20.8	0	0.876	0.417	5.24	
837	1.11	0	0	20.8	0	0.876	0.208	2.81	
365	2.36	0	0	29.1	0	2.01	0	0.286	4.27
365	2.36	0	0	29.1	0	2.01	1.02	4.69	
365	2.36	0	0	29.1	0	2.01	0.815	3.79	
365	2.36	0	0	29.1	0	2.01	0.611	3.00	
365	2.36	0	0	29.1	0	2.01	0.407	2.18	
365	2.36	0	0	29.1	0	2.01	0.204	1.27	
411	2.09	0	0	28.4	0	1.78	0	0.213	3.34
411	2.09	0	0	28.4	0	1.78	1.03	3.75	
411	2.09	0	0	28.4	0	1.78	0.826	2.99	
411	2.09	0	0	28.4	0	1.78	0.619	2.37	
411	2.09	0	0	28.4	0	1.78	0.413	1.62	
411	2.09	0	0	28.4	0	1.78	0.206	1.09	
411	2.09	0	0	28.4	0	1.78	0	0.270	
298	2.27	0	0	30.7	0	2.46	0.307	3.64	10.4
298	2.27	0	0	30.7	0	2.46	0.614	6.94	
298	2.27	0	0	30.7	0	2.46	0	0.505	
298	9.59	0	0	39.8	0	7.36	0	0.925	9.44
298	9.59	0	0	39.8	0	7.36	1.0	10.570	
298	9.59	0	0	39.8	0	7.36	0.8	8.62	
298	9.59	0	0	39.8	0	7.36	0.6	6.76	
298	9.59	0	0	39.8	0	7.36	0.4	4.81	
298	9.59	0	0	39.8	0	7.36	0.2	3.29	
298	9.59	0	0	39.8	0	7.36	0	1.2	
298	13.0	0	0	40.1	0	24.5	0	1.7	4.63
298	13.0	0	0	40.1	0	24.5	1.00	6.25	
298	13.0	0	0	40.1	0	24.5	0.802	5.5	
298	13.0	0	0	40.1	0	24.5	0.601	4.31	
298	13.0	0	0	40.1	0	24.5	0.401	3.41	
298	13.0	0	0	40.1	0	24.5	0.2	2.53	
298	28.9	0	0	39.6	0	73.4	0	3.4	2.98
298	28.9	0	0	39.6	0	73.4	1.0	6.4	
298	28.9	0	0	39.6	0	73.4	0.8	5.8	
298	28.9	0	0	39.6	0	73.4	0.6	5.23	
298	28.9	0	0	39.6	0	73.4	0.4	4.76	
298	28.9	0	0	39.6	0	73.4	0.2	4.18	
298	28.9	0	0	39.6	0	73.4	0	3.44	
298	67.1	0	0	43.8	0	245	0	2.32	4.56
298	67.1	0	0	43.8	0	245	1.09	7.46	
298	67.1	0	0	43.8	0	245	0.884	6.1	
298	67.1	0	0	43.8	0	245	0.664	5.52	
298	67.1	0	0	43.8	0	245	0.44	4.50	
298	67.1	0	0	43.8	0	245	0.22	3.29	
298	67.1	0	0	43.8	0	245	0	2.42	

overall lifetime of OH ($\tau_{decay} > 10\tau_{rise}$). Again, the rate constant was obtained by plotting the decay constant *vs.* TMP concentration.

The results of all measurements where ozone was used as a photolytic source of excited oxygen atoms are listed in Table 1 and shown in Fig. 5. The negative temperature dependence in this temperature range is apparent. The deviation from linear

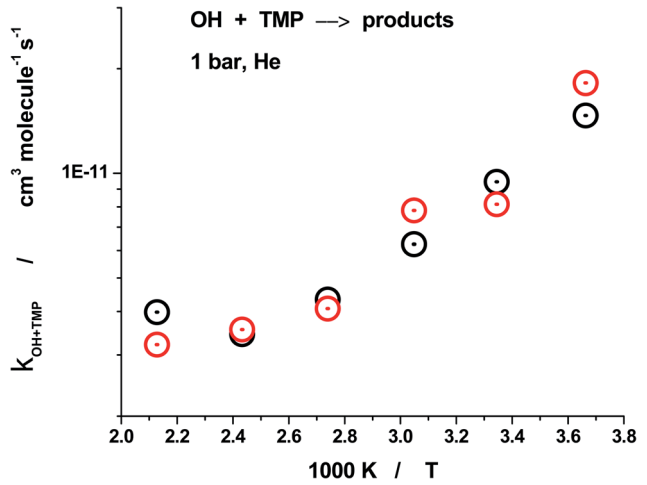

Fig. 5 Summary of the measurements of the rate constant of reaction (1) in the experiments where ozone was used as a photolytical precursor of excited oxygen atoms, $O(^1D)$. Rate constant of reaction (1) at 1 bar, over the temperature range 273–470 K. Black points: O_3/ H_2O + 266 nm, red points: O_3/H_2/He +266 nm.

dependence in the Arrhenius coordinates at the highest temperature achievable when ozone is used to produce excited oxygen atoms (470 K) is also apparent. This deviation suggests possibility of a turning point in the temperature dependence. As it was previously mentioned, the temperature range in the experiments involving ozone was limited by the thermal stability of ozone.

The temperature range of the study was significantly extended by using N_2O as a photolytic source of excited oxygen atoms, $O(^1D)$. N_2O has much better thermal stability, the upper temperature of the experiments was raised to 837 K. Sample decay profiles obtained in the photolysis system N_2O/H_2O/TMP/He + $h\nu$ (193 nm) at 673 K are shown in Fig. 6. Data processing

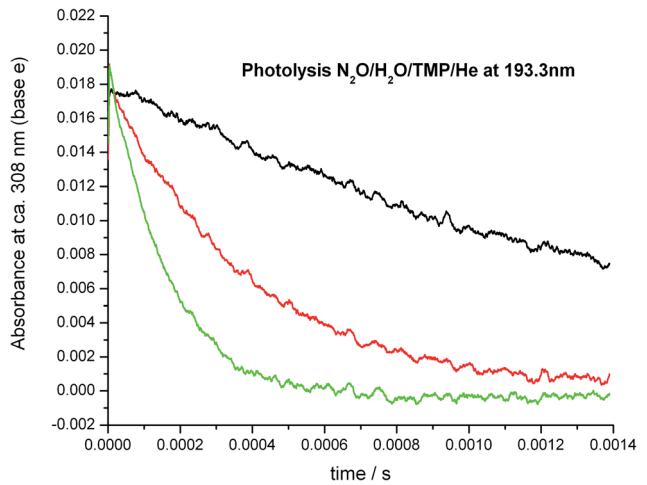

Fig. 6 Sample UV absorption profiles of OH radical (multiline at *ca.* 308 nm). Photolysis of N_2O/H_2O/TMP/He mixtures at 193.3 nm. T = 673 K, p = 1 bar. [N_2O] = 1.66×10^{16} molecules per cm^3, [H_2O] = 3.66×10^{17} molecules per cm^3, [N_2O]/[H_2O] = 0.054, [TMP] = 0–10×10^{14} molecules per cm^3. The initial concentration of OH is approximately the same. Black – [TMP] = 0, red – [TMP] = 4×10^{14} molecules per cm^3, green – [TMP] = 10×10^{14} molecule per cm^3.

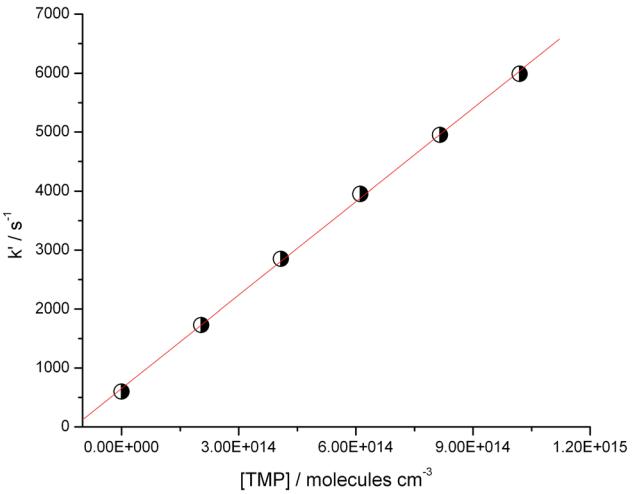

Fig. 7 Sample dependence of the k' determined *via* the "initial slopes" of the decay temporal profiles (at 673 K, 1 bar), *versus* the reactant concentration, [TMP]. The other reactants concentrations were kept constant, except for [TMP] which was varied from 0 to 10×10^{14} molecules per cm^3 in 5 equal increments *via* varying the flow rate of the TMP solution in water. To determine the "initial slope", the portion of the decay profiles that correspond to *ca.* 1/3 drop of the initial amplitude was fitted with an exponential function to determine the k'. Subsequently, the slope of the linear fit of the dependence k' *vs.* [TMP] resulted in the reaction rate constant k_1(TMP + OH).

via plotting the "initial slope" rate constant k' *vs.* concentration of the reactant, TMP, is shown in Fig. 7. Similar plots for all temperatures are shown in Fig. 8. The negative temperature dependence at low temperatures turns to a positive dependence at higher temperatures. All the results (including the experiments with ozone) together with the experimental conditions are summarized in Table 1 and shown in Fig. 9. Current results at room temperature are in excellent agreement with the only previous determination (black star in Fig. 9).

To describe the apparent V-shaped temperature dependence of the rate constant of reaction (1), a 3-parameter modified

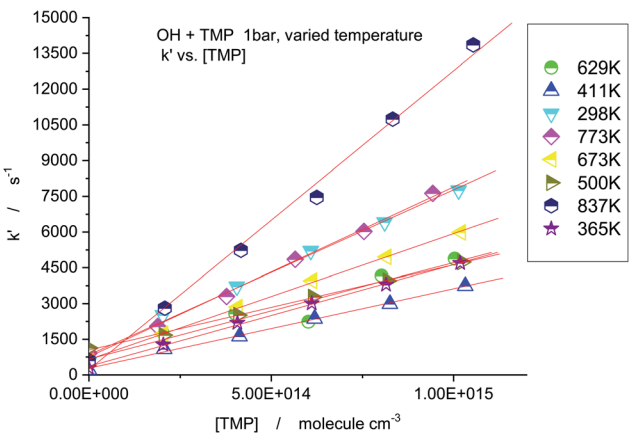

Fig. 8 Summary of k' *vs.* [TMP] at different temperatures. The slopes of the linear fits result in the rate constants k (TMP + OH).

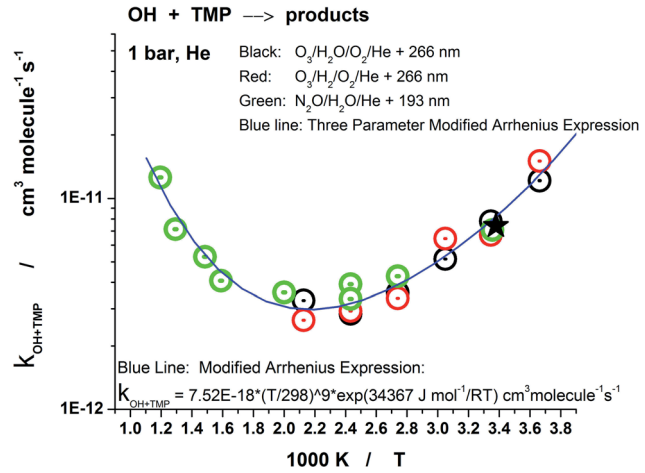

Fig. 9 Summary rate constant of reaction (1) at 1 bar, over the temperature range 273–837 K. Green points: N_2O/H_2O/He + 193 nm, black points: O_3/H_2O + 266 nm, red points: O_3/H_2/He + 266 nm. Blue line – fit by the modified 3-parameter Arrhenius expression (see text). Black star: the only previous experimental measurement (relative rates method[1]).

Arrhenius expression was used. All data could be reasonably fitted by the following expression:

$$k_1 = 7.52 \times 10^{-18}\,(T/298)^9\exp(34\,367\ \text{J mol}^{-1}/\text{RT})\ \text{cm}^3\ \text{per molecule per s (273–837 K)} \quad \text{(E3)}$$

Discussion

The most striking feature is the V-shaped temperature dependence of the rate constant – negative at low temperatures, positive at high temperatures, with the turning point at 471 K. There could be potentially two reasons for such peculiar temperature dependence. One possibility is that the ground state of the transition state lies below the ground state of the reactants ("negative barrier", submerged barrier).[25,26] In such a case the modified transition state theory predicts V-shaped temperature dependence, negative at low temperatures, and positive at high temperatures, with possible pressure dependence at high pressures.[25,26] Another possibility is that the reaction has two or more channels, like direct H-atom abstraction from CH_3 groups as well as attachment of OH to the double P═O bond in TMP:

$$\text{OH} + (\text{CH}_3\text{O})_3\text{PO} \rightarrow \text{H}_2\text{O} + \text{CH}_2(\text{CH}_3)_2\text{PO} \quad \text{(1a)}$$

$$\text{OH} + (\text{CH}_3\text{O})_3\text{PO} \rightarrow (\text{CH}_3\text{O})_3\text{P(OH)O} \rightarrow \text{products} \quad \text{(1b)}$$

The only available theoretical work[15] focuses on the direct abstraction channel (1a), no data on the prospective complex forming channel (1b) with further transformations within the complex are currently available. Complex forming reactions often have negative temperature dependence, typical H-atom abstraction reactions usually have small positive barriers.[27] It should be noted, that theoretical calculation for OH + TMP, resulted in "negative barriers" for several conformers of the transition state, as well as in the negative temperature dependence of the rate constant at low temperatures.[15] When complex formation is involved, significant pressure effects could be expected. Such measurements are currently underway.

Conclusions

The reaction of hydroxyl radical with trimethyl phosphate (reaction (1)) was studied by two groups using three different methods of generation of hydroxyl radicals over an extended temperature range 273–837 K.

The room temperature rate constant is in excellent agreement with the only previous determination.[14]

A V-shaped temperature dependence, negative at low temperatures, and positive at higher temperatures, with a turning point at 471 K, was unambiguously established.

It is apparent that extended experimental (including bath gas pressure dependence) as well at theoretical studies of this reaction, as well as for other phosphorus centered compounds, are required for understanding of the mechanism of these reaction.

Conflicts of interest

There are no conflicts to declare.

Acknowledgements

The study performed at IChK&C (Novosibirsk) was supported by a grant from the Russian Science Foundation (Grant No. 19-73-20060).

References

1 A. N. Baratov, *Monograph*, FSU VNIIPO MINISTRY of Emergency Situations of Russia, 2003, p. 364.
2 R. E. Tapscott, R. S. Sheinson, V. Babushok, M. R. Nyden, and R. G. Gann, Technical Note (NIST TN) - 1443, *Alternative Fire Suppressant Chemicals: A Research Review with Recommendations*, 2001, p. 84.
3 J. W. Hastie and D. W. Bonnell, *Molecular Chemistry of Inhibited Combustion Systems*, National Bureau of Standards, B81-170375, 1980, p. 206, Final NBSIR, 80-2169, B81-170375.
4 A. J. Twarowski, The Influence of Phosphorus Oxides and Acids on Rate of H+OH Recombination, *Combust. Flame*, 1993, **94**, 91–107.
5 A. J. Twarowski, Photometric Determination of the Rate of H2O Formation from H and OH in the Presence of Phosphine Combustion Products, *Combust. Flame*, 1993, **94**, 341–348.
6 A. J. Twarowski, Reduction of a Phosphorus Oxide and Acid Reaction Set, *Combust. Flame*, 1995, **102**, 41–54.
7 A. J. Twarowski, The Temperature Dependence of H+OH Recombination in Phosphorus Oxide Containing Combustion Gases, *Combust. Flame*, 1996, **105**, 407–413.

8 O. P. Korobeinichev, V. M. Shvartsberg and A. A. Chernov, The destruction chemistry of organophosphorus compounds in flames—II: structure of a hydrogen–oxygen flame doped with trimethylphosphate, *Combust. Flame*, 1999, **118**, 727–732.

9 O. P. Korobeinichev, V. M. Shvartsberg, A. A. Chernov, V. V. Mokrushin, Hydrogen-oxygen flame doped with trimethyl phosphate, its structure and trimethyl phosphate destruction chemistry, *Symposium (International) on Combustion*, 1996, vol. 26, pp. 1035–1042.

10 O. P. Korobeinichev, T. A. Bolshova, V. M. Shvartsberg and A. A. Chernov, Inhibition and promotion of combustion by organophosphorus compounds added to flames of CH_4 or H_2 in O_2 and Ar, *Combust. Flame*, 2001, **125**, 744–751.

11 P. A. Glaude, H. J. Curran, W. J. Pitz and C. K. Westbrook, Kinetic study of the combustion of organophosphorus compounds, *Proc. Combust. Inst.*, 2000, **28**, 1749–1756.

12 P. A. Glaude, C. Melius, W. J. Pitz and C. K. Westbrook, Detailed Chemical Kinetic Reaction Mechanisms for Incineration of Organophosphorus and Fluoro-Organophosphorus Compounds, *Proc. Combust. Inst.*, 2002, **29**, 469–2476.

13 T. M. Jayaweera, C. F. Melius, W. J. Pitz, C. K. Westbrook, O. P. Korobeinichev, V. M. Shvartsberg, A. G. Shmakov, I. V. Rybitskaya and H. J. Curran, Flame Inhibition by Phosphorus-Containing Compounds over a Range of Equivalence Ratios, *Combust. Flame*, 2005, **140**, 103–115.

14 E. C. Tuazon, R. Atkinson, S. M. Aschumann, J. Arey, A. M. Winer and J. N. Pitts Jr, Atmospheric Loss Processes of 1,2-Dibromo-3-Chloropropane and Trimethyl Phosphate, *Environ. Sci. Technol.*, 1986, **20**, 1043–1046.

15 D. S. Burns, M. G. Cory, D. E. Taylor, S. W. Bunte, K. Runge and J. L. Vasey, A Comparison of Primary and Secondary Hydrogen Abstraction from Organophosphates by Hydroxyl Radical, *Int. J. Chem. Kinet.*, 2013, **45**, 187–201.

16 E. J. Dunlea and A. R. Ravishankara, Measurement of the Rate Coefficient for the Reaction of $O(^1D)$ with H_2O and Re-Evaluation of the Atmospheric OH Production Rate, *Phys. Chem. Chem. Phys.*, 2004, **6**, 3333–3340.

17 X. Zhang, M. Sangwan, C. Yan, P. V. Koshlyakov, E. N. Chesnokov, Y. Bedjanian and L. N. Krasnoperov, Disproportionation Channel of the Self-reaction of Hydroxyl Radical, OH + OH → H 2 O + O, Revisited, *J. Phys. Chem. A*, 2020, **124**, 3993–4005.

18 M. Sangwan and L. N. Krasnoperov, Disproportionation Channel of Self-Reaction of Hydroxyl Radical, OH + OH → H_2O + O, Studied by Time-Resolved Oxygen Atom Trapping, *J. Phys. Chem. A*, 2012, **116**, 11817–11822.

19 M. Sangwan, E. N. Chesnokov and L. N. Krasnoperov, Reaction OH + OH Studied over the 298–834 K Temperature and 1 - 100 bar Pressure Ranges, *J. Phys. Chem. A*, 2012, **116**, 6282–6294.

20 C. Yan, S. Kocevska and L. N. Krasnoperov, Kinetics of the Reaction of CH3O2 Radicals with OH Studied over the 292–526 K Temperature Range, *J. Phys. Chem. A*, 2016, **120**, 6111–6121.

21 M. Sangwan and L. N. Krasnoperov, Kinetics of the Gas Phase Reaction CH_3 + HO_2, *J. Phys. Chem. A*, 2013, **117**, 2916–2923.

22 M. Sangwan, C. Yan, E. N. Chesnokov and L. N. Krasnoperov, Reaction $CH_3 + CH_3 \rightarrow C_2H_6$ Studied over the 292 -714 K and 1 – 100 bar Pressure Ranges, *J. Phys. Chem. A*, 2015, **119**, 7847–7857.

23 M. Sangwan, E. N. Chesnokov and L. N. Krasnoperov, Reaction CH3 + OH Studied over the 294 - 714 K Temperature and 1 - 100 bar Pressure Ranges, *J. Phys. Chem. A*, 2012, **116**, 8661–8670.

24 A. P. Force and J. R. Wiesenfeld, Laser Photolysis of O3/H2 Mixtures: The Yield of the H + O3 → HO2 + O Reaction, *J. Chem. Phys.*, 1981, **74**, 1718–1723.

25 L. N. Krasnoperov, J. Peng and P. Marshall, Modified Transition State Theory and Negative Apparent Activation Energies of Simple Metathesis Reactions: Application to the Reaction CH_3 + HBr → CH_4 + Br, *J. Phys. Chem. A*, 2005, **110**, 3110–3120.

26 Y. Gao, I. M. Alecu, P.-C. Hsieh, B. P. Morgan, P. Marshall and L. N. Krasnoperov, Thermochemistry Is Not a Lower Bound to the Activation Energy of Endothermic Reactions: A Kinetic Study of the Gas-Phase Reaction of Atomic Chlorine with Ammonia, *J. Phys. Chem. A*, 2006, **110**, 6844–6850.

27 J. A. Manion; R. E. Huie; R. D. Levin; Jr., D. R. B.; V. L. Orkin; W. Tsang; W. S. McGivern; J. W. Hudgens; V. D. Knyazev; D. B. Atkinson, *et al.*, NIST Chemical Kinetics Database, NIST Standard Reference Database 17, Version 7.0 (Web Version), Release 1.4.3, Data version 2008.12, National Institute of Standards and Technology, Gaithersburg, Maryland, 20899-8320. Web address: http://kinetics.nist.gov/.2008.